Water Gauge Image Denoising Model Based on Improved Adaptive Total Variation

SHI Zhenting[1], ZHOU Xianchun[2], ZHANG Ying[3], LI Ting[3], LU Siqi[3]

(1. *School of Electronic and Information Engineering*, *Nanjing University of Information Science and Technology*, *Nanjing 210044*; 2. *School of Artificial Intelligence*, *Nanjing University of Information Science and Technology*, *Nanjing 210044*; 3. *School of Electronic and Information Engineering*, *Nanjing University of Information Science and Technology*, *Nanjing 210044*)

Abstract: As an important part of water level warning in water conservancy projects, often due to the influence of environmental factors such as light and stains, the acquired water gauge images have sticky, broken and bright spot conditions, which affect the identification of water gauges. To solve this problem, a water gauge image denoising model based on improved adaptive total variation is proposed. Firstly, the regular term exponent in the adaptive total variational equation is changed to an inverse cosine function; secondly, the differential curvature is used to distinguish the image noise points and increase the smoothing strength at the noise points; finally, according to the characteristics of the gradient mode and adaptive gradient threshold after Gaussian filtering, the New model can adaptively denoise in the smooth area and protect the edge area, so as to have the characteristics of both edge-preserving denoising. The experimental results show that the new model has a great improvement in image vision, higher iteration efficiency and an average increase of 1.6 dB in peak signal-to-noise ratio, and an average increase of 9% in structural similarity, which is more beneficial to practical applications.

Keywords: Water Gauge Image, Adaptive Total Variation, Differential Curvature, Gradient Mode, Adaptive Gradient Threshold

1 Introduction

In water and rainfall monitoring and early warning systems, the use of images to identify the scale of water rulers and collect water levels has become a development trend[1]. Due to the complex reasons such as the changeable surrounding environment, the collected water gauge images are susceptible to noise and the readings are not easy to observe. Therefore, it is necessary to denoise the water gauge images by digital image processing techniques. Currently, traditional image denoising methods[2] can be divided into filter transform-based denoising methods and partial differential equation-based denoising methods. Among the filter transform-based denoising methods, the spatial domain filtering method scatters the noise around the pixels, resulting in a larger noise coverage area and easy loss of abrupt phase change information[3]. Moreover, the frequency domain filtering method does not retain the texture details of the image better and is influenced by the choice of filters[4]. Therefore, the denoising methods based on partial differential equations have caused a boom. In the 1970s, Tikhonov proposed the ℓ2 norm-based reconciliation model, which cannot protect the edges of the image and has severe loss of texture details. In 1992, Rudin, Oster and Fatemi proposed the

Total Variation (TV) model, which replaces the ℓ2 norm in the reconciliation model with the ℓ1 norm to better protect the edges of the image, but is prone to the "staircase effect" in the smooth area. To solve this problem, researchers have proposed many improvements[5-9]. Bing Song proposed a TV denoising model based on ℓp norm, which can effectively suppress the "staircase effect", but the selection of parameters is relatively strict and lacks generality. In view of this, Zhang et al[10] proposed an adaptive TV denoising model, the ZTV model, which can adaptively select the value of parameter p to effectively suppress the "staircase effect" and achieve the effect of edge-preserving denoising. Bredies et al[11] proposed a generalized Total Generalized Variation (TGV) model, which applies higher order discrete gradient operators to image denoising, but the complexity of the iterative algorithm is high and the convergence speed is slow. You and Kaveh[12] proposed a second-order Laplace model for denoising, which can effectively suppress the "staircase effect", but causes edge blurring. Chen et al[13]. proposed a weighted group sparse regularized low-rank tensor decomposition model, which uses the weighted ℓ2,1 norm to constrain the differential images, which further improves the denoising effect.

In the reference[14], a new weighted total variational model was proposed to effectively suppress the "staircase effect" and protect the texture information of images. In recent years, deep learning-based denoising methods[15-16]have been widely used, which can achieve better denoising effects, but with long running time, high hardware cost and complex models.

In this paper, a water gauge image denoising model based on improved adaptive total variation based on the ℓ1 norm-based TV model combined with the ℓp norm is proposed. Firstly, the regular term exponent in the total variational equation is changed to an inverse cosine function; secondly, the differential curvature[17-18] is used to distinguish the image noise points; finally, combining the properties of the Gaussian filtered gradient mode and the adaptive gradient threshold derived from the median absolute deviation[19-20], the New model achieves different denoising effects in different areas. Compared with various total variation denoising models, the New model not only improves in image vision, but also improves PSNR, SSIM and iteration efficiency.

2 Classical Total Variational Image Denoising Model

This paper uses u to denote the denoised image, v to denote the noisy image, u_0 to denote the original image and w to denote the noise.

Then the noise model of the image can be obtained as shown in equation (1):

$$v = u_0 + w \tag{1}$$

2.1 Reconciliation Model Based ℓ2 Norm

In this paper, the ℓ2-TV model is used instead of the reconciliation model based ℓ2 norm, then the ℓ2-TV model is shown in equation (2):

$$\begin{cases} \dfrac{\partial u}{\partial t} = \nabla \cdot (\nabla u) - \lambda (u - v) \\ u(x, y, t)\big|_{t=0} = v(x, y) \end{cases} \tag{2}$$

In formula (2), ∇ is the gradient operator; λ is the weight coefficient, the model is an isotropic diffusion model, which is easy to make the edge part blurred in the denoising process.

2.2 TV Denoising Model Based ℓ1 Norm

In this paper, the ℓ1-TV model is used instead of the TV denoising model based on the ℓ1 norm, and then the ℓ1-TV model is shown in equation (3):

$$\begin{cases} \dfrac{\partial u}{\partial t} = \nabla \cdot \left(\dfrac{\nabla u}{|\nabla u|}\right) - \lambda (u - v) \\ u(x, y, t)\big|_{t=0} = v(x, y) \end{cases} \tag{3}$$

This model is an anisotropic diffusion model, which can effectively protect the edges of the image. However, in the smooth area, it is easy to treat the noise as an edge and produce the phenomenon of "staircase effect".

2.3 ZTV Model

The ZTV model is shown in equation (4):

$$\begin{cases} \dfrac{\partial u}{\partial t} = \nabla \cdot \left(\dfrac{\nabla u}{|\nabla u|^{2-p}}\right) - \lambda (u - v) \\ u(x, y, t)\big|_{t=0} = v(x, y) \end{cases} \tag{4}$$

In formula (4), $p(x,y)$ is the control parameter function, related to the gradient information of the image, whose expression is shown in equation (5):

$$p(x,y)=1+\frac{1}{1+\left|\nabla G_\sigma * v(x,y)\right|^2} \tag{5}$$

In formula (5), $*$ is the convolution operator; G_σ is a Gaussian kernel function with standard deviation $\sigma(\sigma>0)$ to pre-smooth the image. In the edge area, $\left|\nabla G_\sigma * v(x,y)\right|$ is larger, $p\to 1$, the image is denoised by ℓ1-TV model to protect the image edge; In the smooth area, $\left|\nabla G_\sigma * v(x,y)\right|$ is smaller, $p\to 2$, the image is denoised by ℓ2-TV model to remove the noise better.

ZTV model has the advantages of ℓ1-TV model and ℓ2-TV model, but the denoising index of this model still needs to be improved.

3 New Model

The energy generalized expression of the new model is shown in equation (6):

$$\min_u E_2(u)=\frac{1}{p}\iint_\Omega |\nabla u|_\varepsilon^p dxdy+\frac{\lambda}{2}\iint_\Omega |u-v|^2 \mathrm{d}x\mathrm{d}y \tag{6}$$

In formula (6), the first term is the regular term and the second term is the fidelity term; λ is the weight coefficient, which can adaptively adjust the weights of the regular and fidelity terms; $|\nabla u|$ is the gradient modulus of the denoised image; $|\nabla u|_\varepsilon=\sqrt{|\nabla u|^2+\varepsilon^2}$, ε is a very small value, which regularize $|\nabla u|$ to avoid being zero.

Using the gradient descent method, the partial differential equation corresponding to its Euler-Lagrange equation can be obtained as shown in equation (7):

$$\begin{cases}\dfrac{\partial u}{\partial t}=\nabla\cdot\left(\dfrac{\nabla u}{|\nabla u|_\varepsilon^{2-p}}\right)-\lambda(u-v)\\ u(x,y,t)\big|_{t=0}=v(x,y)\end{cases} \tag{7}$$

Using the finite difference method to find the discrete equation corresponding to equation (7), which is shown in equation (8):

$$\begin{aligned}u_{i,j}^{m+1}&=u_{i,j}^m-\Delta t\times\lambda_m\times(u_{i,j}^m-v(i,j))\\&+\Delta t\times\nabla\cdot\left(\frac{\nabla u_{i,j}^m}{|\nabla u_{i,j}^m|_\varepsilon^{2-p}}\right)\end{aligned} \tag{8}$$

In formula (8), $u_{i,j}$ is the grayscale value of image u at pixel point (x_i,y_j); $u_{i,j}^m$ is the value of $u(x_i,y_j,t_m)$ at m iterations; $t_m=m\Delta t$; λ_m is the value of λ at m iterations; p is the regular term index.

The λ_m expression is shown in equation (9):

$$\lambda_m=\frac{\Sigma\left(\nabla\cdot\left(\dfrac{\nabla u_{i,j}^m}{|\nabla u_{i,j}^m|_\varepsilon^{2-p}}\right)\times(u_{i,j}^m-v(i,j))\right)}{W\times H\times\sigma_m^2} \tag{9}$$

In formula (9), σ_m is the standard deviation of the noise for m iterations, then the expression is shown in equation (10):

$$\sigma_m=\sqrt{\frac{\pi}{2}}\times\frac{\Sigma|v(i,j)*N|}{6\times(W-2)\times(H-1)} \tag{10}$$

In formula (10), N is the difference between two different Laplace filters; $|v(i,j)*N|$ is the modulus of the difference made by two different Laplace filters after filtering the noisy image, and W and H are the values of the rows and columns of the image after Laplace filtering, respectively.

The expression for the regular term index p is shown in equation (11):

$$p=\begin{cases}2 & dc<0.01\\ 1+\dfrac{2}{\pi}\operatorname{arccot}\left(b\cdot\left(\dfrac{|\nabla G_\sigma * u|}{k}\right)^2\right) & dc\geqslant 0.01\end{cases} \tag{11}$$

In formula (11), k is the adaptive gradient threshold. It is derived adaptively by the Median Absolute Deviation (MAD) of the gradient in the current neighborhood. The expression is shown in equation (12):

$$k=\frac{med(\|\nabla G_\sigma * u|-med(|\nabla G_\sigma * u|)\|)}{0.6745} \tag{12}$$

In formula (12), the constant is set to 1/0.6745 because the MAD of a normal distribution with a mean of 0 and a variance of 1 is 1/0.6745.

The expression of the coefficient b is shown in equation (13):

$$b=\begin{cases}e^{|\nabla G_\sigma * u|} & |\nabla G_\sigma * u|\geqslant k\\ 1 & |\nabla G_\sigma * u|<k\end{cases} \tag{13}$$

dc is the normalized differential curvature and its expression is shown in equation (14):

$$dc = \frac{DC - \min(DC)}{\max(DC) - \min(DC)} \tag{14}$$

In formula (14)

$$DC = \left\| u_{\eta\eta} \right| - \left| u_{\varsigma\varsigma} \right\| \tag{15}$$

In formula (15), $|\mu_{\eta\eta}|$ is the second-order derivative of the image along the gradient direction and $|\mu_{\zeta\zeta}|$ is the second-order derivative of the image along the edge direction. The expressions are shown in equations (16) and (17):

$$u_{\eta\eta} = \frac{u_{xx}u_x^2 + 2u_{xy}u_x u_y + u_{yy}u_y^2}{u_x^2 + u_y^2} \tag{16}$$

$$u_{\varsigma\varsigma} = \frac{u_{xx}u_y^2 - 2u_{xy}u_x u_y + u_{yy}u_x^2}{u_x^2 + u_y^2} \tag{17}$$

In the edge area, $|\mu_{\zeta\zeta}|$ is small and $|\mu_{\eta\eta}|$ is large, so the DC value is large; in the smooth area, both $|\mu_{\zeta\zeta}|$ and $|\mu_{\eta\eta}|$ are small, so the DC value is small; at the isolated noise point, both $|\mu_{\zeta\zeta}|$ and $|\mu_{\eta\eta}|$ are large and almost equal, so the DC value is small and approximated to 0.

Therefore, in this paper, the threshold of normalized difference curvature can be set to 0.01 to distinguish the image at the isolated noise point, the smooth area and the edge area.

When $dc < 0.01$ 1, at this time at the isolated noise point, p=2, the image is denoised by ℓ2-TV model, which can effectively remove the isolated noise point.

When $dc \geqslant 0.01$, $p = 1 + \frac{2}{\pi}\operatorname{arccot}(b \cdot (\frac{|\nabla G_\sigma * u|}{k})^2)$.

If $|\nabla G_\sigma * u|$ is small, $b \cdot (\frac{|\nabla G_\sigma * u|}{k})^2 \to 0$, $p \to 2$, at this time, in the smooth area, ℓ2-TV model denoising is performed, which can effectively remove the noise; if is larger, $b \cdot (\frac{|\nabla G_\sigma * u|}{k})^2 \to \infty$, $p \to 1$, at this time, in the edge area, ℓ1-TV model denoising is performed, which can effectively protect the image edges. Coefficients $b = e^{|\nabla G_\sigma * u|}$ are introduced in order to speed up the $p \to 1$ in the edge area and to protect the image edges more effectively.

Therefore, at isolated noise points, $p = 2$, ℓ2-TV model denoising is performed; in the edge area, $p \to 1$, ℓ1-TV model denoising is performed; in the smooth area, , ℓ2-TV model denoising is performed; therefore, the New model has the advantage of both edge-preserving denoising and good flexibility.

The algorithm implementation steps of the new model are as follows:

1. Initialization: according to equation (9) to find out λ, according to equation (21) to find out the number of iterations, while setting the value of the time step Δt.

2. Start the iteration: Calculate the value of k, dc and b. Bring the Gaussian filtered gradient modulus value, k, dc and b into equation(11) to find the value of p. Bringing λ, Δt and p into the discrete model of equation (8), the iteration is performed.

3. Until the number of iterations N satisfies the condition, take the PSNR value corresponding to the New model.

---

4 Experimental Results and Analysis

In order to verify the effectiveness of the New model, as shown in Fig.1, four grayscale images of water gauge with size 256×256 pixels, one image of woman face with size 256×256 pixels and one image of butterfly with size 256×256 pixels, a total of six images, are selected as the test images. On this basis, Gaussian white noise with standard deviations of 20, 25, 30 and 35 is added. The noise image (σ=35) is shown in Fig.2. The denoising effect of the new model is compared with the ℓ2-TV model, ℓ1-TV model and ZTV model to verify the effectiveness of the new model. Meanwhile, Peak Signal-to-Noise Ratio (PSNR) and Structural Similarity Index Measurement (SSIM) are used to measure the image quality after denoising, and then combined with the calculation time t, the denoising effect of new model is analyzed comprehensively. The operating system of the experimental platform is Windows 11, and the programming environment is Matlab R2018b.

The PSNR expression is shown in equation (18):

$$PSNR = 10 \times \log_{10}(\frac{(2^n - 1)^2}{MSE}) \tag{18}$$

In formula (18)

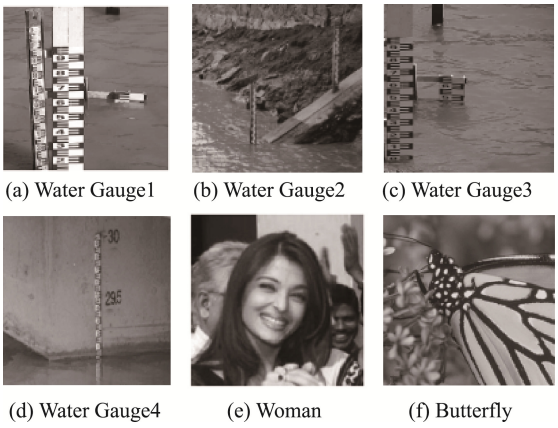

Fig.1 The Original Images

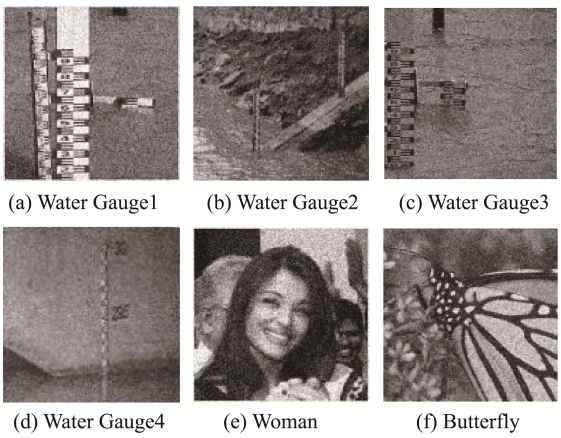

Fig.2 Noise Images

$$MSE = \frac{1}{m \times n} \sum_{i=0}^{m-1} \sum_{j=0}^{n-1} \left\| u(i,j) - u_0(i,j) \right\|^2 \qquad (19)$$

In formula (19)

$m \times n$ is the image size, $u_0(i,j)$ is the original image and $u(i,j)$ is the denoised image.

The SSIM expression is shown in equation (20):

$$SSIM = \frac{(2\mu_{u_0}\mu_u + c_1)(\sigma_{u_0 u} + c_2)}{(\mu_{u_0}^2 + \mu_u^2 + c_1)(\sigma_{u_0}^2 + \sigma_u^2 + c_2)} \qquad (20)$$

In formula (20), μ_{u_0} is the mean of u_0, μ_u is the mean of u, σ_u^2 is the variance of u_0, σ_u^2 is the variance of u, $\sigma_{u_0 u}$ is the covariance of u_0 and u.

4.1 Experimental Qualitative Analysis

The Water gauge 1, Water gauge 3, Water gauge 4 and Woman with the noise standard deviation σ=35 were added as the research objects, and ℓ2-TV model, ℓ1-TV model, ZTV model and new model were used for the denoising process.

4.1.1 Analysis from the Overall Perspective

In each sub-picture of Fig.3 to Fig.6, the right sub-picture is a local enlargement of the left sub-picture.

From Fig.3 to Fig.6, it can be seen that the ℓ2-TV model has the worst effect, with poor edge protection and serious loss of detail texture and unclear contour of the image; the ℓ1-TV model and ZTV model have the second best denoising effect, both the ℓ1-TV model and ZTV model have more noise points and the image is blurrier; the New model has the best denoising effect, with obvious detail features and contour of the image and better visual effect of the image, which is closer to the original image.

4.1.2 Analysis of the Denoising Effect and Edge Protection Effect from the Enlarged Local Image

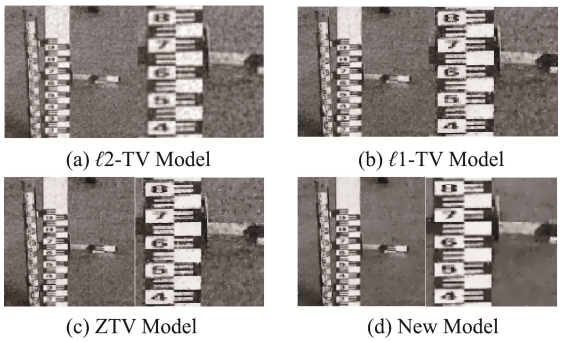

Fig.3 Water Gauge 1 Image Comparison of Denoising Effects Using Four Models

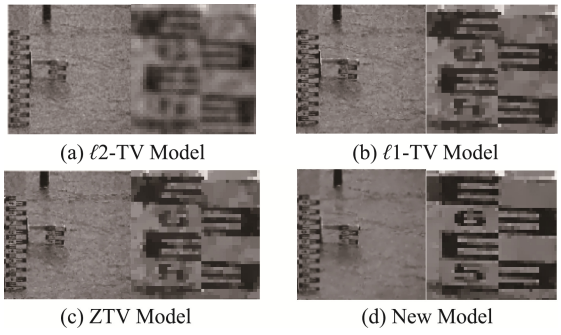

Fig.4 Water Gauge 3 Image Comparison of Denoising Effects Using Four Models

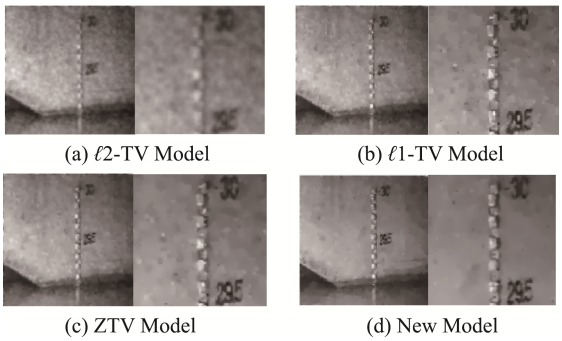

(a) $\ell 2$-TV Model (b) $\ell 1$-TV Model

(c) ZTV Model (d) New Model

Fig.5 Water Gauge 4 Image Comparison of Denoising Effects Using Four Models

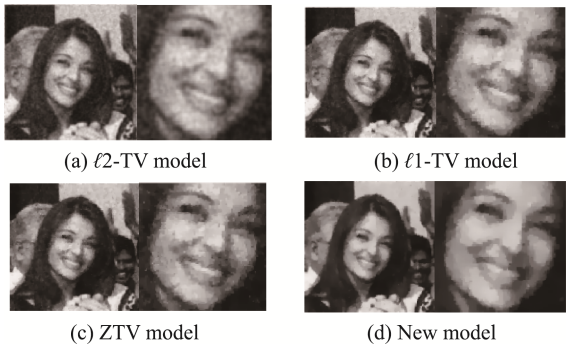

(a) $\ell 2$-TV model (b) $\ell 1$-TV model

(c) ZTV model (d) New model

Fig.6 Woman Image Comparison of Denoising Effects Using Four Models

From Fig.3 to Fig.5, it can be seen that the denoising of $\ell 2$-TV model is not complete, and the numbers on the water gauge image are blurred; there are more isolated noise points in the processing effect image of $\ell 1$-TV model, and the water gauge image is not clear. In the processing result image of ZTV model, there are still isolated noise points, and the clarity is low. Observation of the New model denoising effect image, it did not appear obvious image blurring and more noise points, can clearly see the water gauge image of the numbers, denoising effect is significantly higher than the other three total variation models.

As can be seen from Fig.6, the local image of Woman in the $\ell 2$-TV model is blurred; the local image of Woman in the $\ell 1$-TV model has an obvious "staircase effect" and the denoised image is blurred; The ZTV model also has the "staircase effect" and the image boundary is not clear; Observing the denoising effect of the New model, the Woman local image does not have obvious blurring phenomenon and "staircase effect", and the edge contour is clear, so the New model has better edge protection effect.

4.2 Experimental Quantitative Analysis

As can be seen from Table 1, in the image denoising process, as the noise intensity increases, the number of iterations when the image reaches the maximum PSNR also increases. In order to make the denoised image contour clearer and the visual effect better, through several experiments, this paper comes up with a fitting function for the noise standard deviation and the number of iterations as shown in equation (21):

$$N = 8.61 + 3.87 \times (\sigma - 10), \sigma \in (10, 75) \qquad (21)$$

In formula (21), when σ=20, N=48; when σ=25, N=67; when σ=30, N=87; when σ=35, N=106; therefore, in this paper, N is set to the four values of 48, 67, 87 and 106, and Δt is set to 0.2.

Table 2 to Table 7 give a comparison of the denoising effects of the $\ell 2$-TV model, $\ell 1$-TV model, ZTV model and new model after adding Gaussian white noise with standard deviations of 20, 25, 30 and 35 for Water gauge 1, Water gauge 2, Water gauge 3, Water gauge 4, Woman and Butterfly plots, respectively. Two metrics, PSNR and SSIM, are used to quantitatively evaluate the denoised images, and the performance of the denoised models is analyzed comprehensively with the computation time t.

From Table 2 to Table 7, it can be seen that when changing the value of the noise standard deviation, the new model improves the PSNR by 1.32 dB to 2.17 dB and the SSIM by 3% to 19% after denoising compared with the other three models. Therefore, the new model has a better denoising effect.

From the computation time t in Table 2 to Table 7, it can be seen that although the computation time of the $\ell 2$-TV model is shorter, the computation time of the new model is only 1.3 times that of the $\ell 2$-TV model, which is shorter than that of the ZTV model. Therefore, while ensuring the basic denoising effect, the new model should require less computation time by combining both PSNR and SSIM metrics. Therefore, the new model has higher denoising efficiency.

In order to further verify the denoising perfor-

mance of the new model, the performance analysis of the denoising results with PSNR values under different noise standard deviations, and the experimental result is shown in Fig.7. From Fig.7, it can be seen that the new model has the highest PSNR value in the processing effect image compared with the other three models. Once again, the denoising performance of the new model is confirmed.

Table 1 The Number of Iterations N at Reaching the Maximum PSNR for 6 Images with Different Noise Standard Deviations (σ)

Image	Number of Iterations/N						
	σ=10	σ=15	σ=20	σ=25	σ=30	σ=35	σ=40
Water Gauge 1	13	24	38	51	64	77	94
Water Gauge 2	8	18	34	46	67	94	108
Water Gauge 3	12	26	43	53	74	109	123
Water Gauge 4	15	29	46	56	78	114	128
Woman	11	27	44	54	75	111	124
Butterfly	10	21	30	49	70	101	117
Maximum Value	15	29	46	56	78	114	128

Table 2 Comparison of PSNR, SSIM and t after Denoising Using Four Models for the Water Gauge 1 Image

σ	PSNR/dB				SSIM				Calculation Time (t/s)			
	ℓ2-TV	ℓ1-TV	ZTV	New	ℓ2-TV	ℓ1-TV	ZTV	New	ℓ2-TV	ℓ1-TV	ZTV	New
20	23.16	26.93	27.09	29.71	0.65	0.70	0.72	0.88	0.96	1.01	1.14	0.99
25	22.54	25.47	25.60	27.77	0.58	0.65	0.67	0.85	1.02	1.15	1.26	1.21
30	21.87	24.14	24.26	26.30	0.52	0.60	0.62	0.82	1.07	1.09	1.38	1.37
35	21.23	23.14	23.23	25.08	0.47	0.56	0.57	0.79	1.01	1.13	1.46	1.42
Average	22.20	24.92	25.05	27.22	0.56	0.63	0.65	0.84	1.02	1.10	1.31	1.25

Table 3 Comparison of PSNR, SSIM and t after Denoising Using Four Models for the Water Gauge 2 image

σ	PSNR/dB				SSIM				Calculation Time (t/s)			
	ℓ2-TV	ℓ1-TV	ZTV	New	ℓ2-TV	ℓ1-TV	ZTV	New	ℓ2-TV	ℓ1-TV	ZTV	New
20	27.35	26.76	26.89	28.79	0.76	0.74	0.75	0.82	0.92	0.96	1.12	1.11
25	26.61	25.78	25.87	27.41	0.72	0.70	0.71	0.75	0.97	1.06	1.33	1.29
30	25.87	25.13	25.22	26.33	0.69	0.66	0.68	0.69	1.02	1.11	1.49	1.43
35	25.29	24.78	24.83	25.53	0.66	0.63	0.64	0.65	1.08	1.20	1.66	1.64
Average	26.28	25.61	25.70	27.02	0.71	0.68	0.70	0.73	0.99	1.08	1.40	1.37

Table 4 Comparison of PSNR, SSIM and t after Denoising Using Four Models for the Water Gauge 3 Image

σ	PSNR/dB				SSIM				Calculation Time (t/s)			
	ℓ2-TV	ℓ1-TV	ZTV	New	ℓ2-TV	ℓ1-TV	ZTV	New	ℓ2-TV	ℓ1-TV	ZTV	New
20	24.92	27.31	27.44	29.31	0.60	0.69	0.71	0.80	0.98	1.03	1.20	1.18
25	24.12	26.25	26.36	27.80	0.54	0.65	0.66	0.75	1.03	1.07	1.35	1.31
30	23.23	25.24	25.36	26.68	0.48	0.60	0.61	0.71	1.04	1.11	1.49	1.45
35	22.70	24.52	24.59	25.73	0.49	0.57	0.58	0.67	1.06	1.25	1.73	1.70
Average	23.74	25.83	25.94	27.38	0.53	0.63	0.64	0.73	1.03	1.12	1.44	1.41

Table 5 Comparison of PSNR, SSIM and t after Denoising Using Four Models for the Water Gauge 4 Image

σ	PSNR/dB				SSIM				Calculation Time (t/s)			
	ℓ2-TV	ℓ1-TV	ZTV	New	ℓ2-TV	ℓ1-TV	ZTV	New	ℓ2-TV	ℓ1-TV	ZTV	New
20	30.70	32.28	32.49	34.18	0.80	0.82	0.84	0.88	1.03	1.12	1.52	1.51
25	29.99	31.23	31.41	32.73	0.79	0.81	0.82	0.86	1.08	1.32	1.95	1.79
30	29.43	30.39	30.55	31.71	0.78	0.79	0.81	0.85	1.28	1.37	2.01	1.96
35	29.01	29.76	29.90	30.87	0.77	0.78	0.79	0.83	1.33	1.45	2.17	2.13
Average	29.78	30.92	31.09	32.37	0.79	0.80	0.81	0.86	1.18	1.32	1.91	1.85

Table 6 Comparison of PSNR, SSIM and t after Denoising Using Four Models for Woman Image

σ	PSNR/dB				SSIM				Calculation Time (t/s)			
	ℓ2-TV	ℓ1-TV	ZTV	New	ℓ2-TV	ℓ1-TV	ZTV	New	ℓ2-TV	ℓ1-TV	ZTV	New
20	27.83	29.59	29.76	31.75	0.83	0.81	0.83	0.90	0.97	1.05	1.31	1.18
25	27.08	28.49	28.63	30.16	0.79	0.80	0.80	0.87	0.99	1.16	1.45	1.32
30	26.21	27.43	27.54	29.02	0.74	0.76	0.78	0.85	1.06	1.18	1.65	1.49
35	25.48	26.61	26.69	27.85	0.74	0.75	0.75	0.82	1.09	1.28	1.79	1.67
Average	26.65	28.03	28.16	29.70	0.78	0.78	0.79	0.86	1.03	1.17	1.55	1.41

Table 7 Comparison of PSNR, SSIM and t after Denoising Using Four Models for Butterfly Image

σ	PSNR/dB				SSIM				Calculation Time (t/s)			
	ℓ2-TV	ℓ1-TV	ZTV	New	ℓ2-TV	ℓ1-TV	ZTV	New	ℓ2-TV	ℓ1-TV	ZTV	New
20	26.87	28.57	28.76	31.02	0.74	0.82	0.83	0.92	0.95	0.99	1.25	1.18
25	25.75	27.15	27.31	29.49	0.77	0.78	0.79	0.90	1.01	1.06	1.37	1.34
30	25.13	26.34	26.46	28.13	0.73	0.76	0.77	0.87	1.03	1.12	1.63	1.58
35	24.57	25.50	25.61	27.15	0.70	0.73	0.74	0.85	1.04	1.19	1.66	1.65
Average	25.58	26.89	27.04	28.95	0.74	0.77	0.78	0.89	1.01	1.09	1.48	1.44

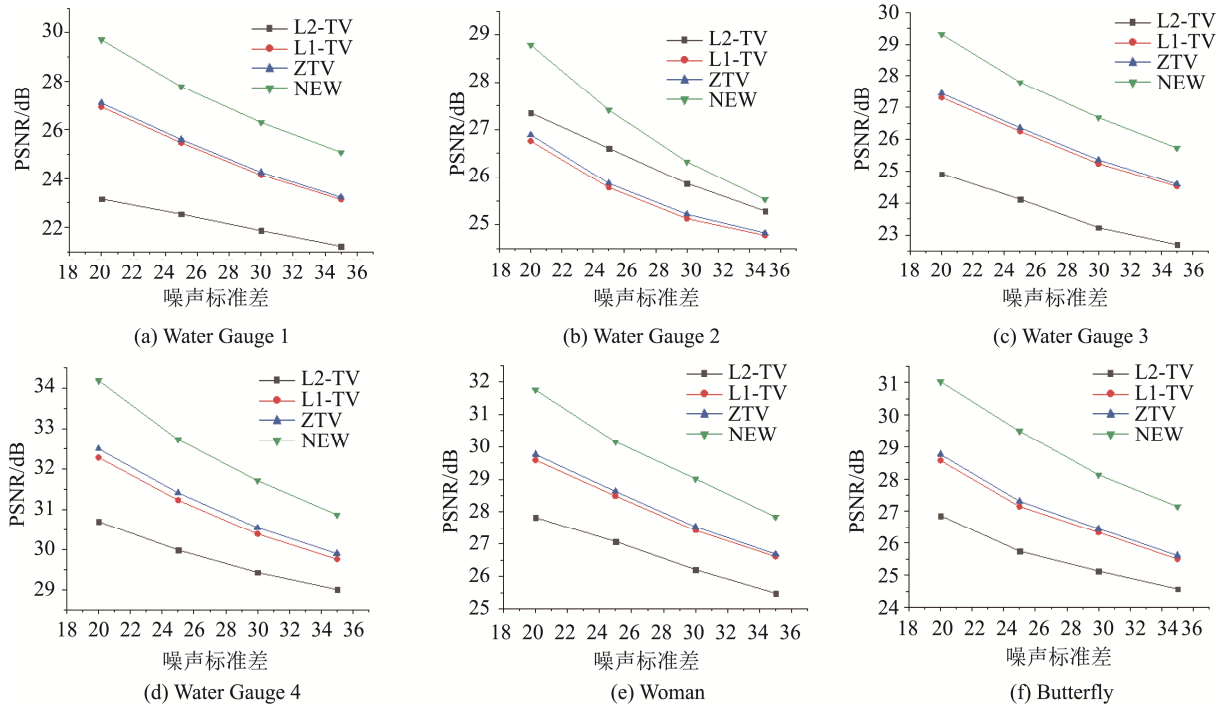

(a) Water Gauge 1 (b) Water Gauge 2 (c) Water Gauge 3

(d) Water Gauge 4 (e) Woman (f) Butterfly

Fig.7 PSNR at Different Noise Standard Deviations for the Four Models

5 Conclusion

The water gauge is used as the core part in water level warning. Due to complex factors such as environment, the collected water gauge images may have blurred conditions. To solve this problem, a water gauge image denoising model based on improved adaptive total variation is proposed. The New model first changes the regular term exponent in the total variance equation to an inverse cosine function, followed by a differential curvature distinction to distinguish the noise points, and then the new model can adaptively smooth the noise in the smooth area and protect the edge area according to the properties of the gradient mode and adaptive gradient threshold after Gaussian filtering. The experimental results show that when denoising images with different noise standard deviations, the New model has a better denoising effect compared with the $\ell 2$-TV model, $\ell 1$-TV model and ZTV model, significantly alleviates the image blur, well preserves the edge details of the image, and greatly improves the visual quality of the denoised image, and the PSNR is improved by 1.6 dB on average and the SSIM is improved by 9%.

References

[1] Dou G, Chen R, Han C, et al. (2022). Research on water-level recognition method based on image processing and convolutional neural networks. Water, 14(12), pp.1890-1916.

[2] Knaus C, Zwicker M. (2015). Dual-domain filtering. SIAM Journal on Imaging Sciences, 8(3), pp. 1396-1420.

[3] Jiang W L, Li G L, Luo W B. (2011). Application of improved median filtering algorithm to image denoising. Journal of Applied Optics, 32(4), pp.678-682.

[4] LI Y W. (2016). Research on video image frame recovery technology based on frequency domain filtering. Electronic Measurement Technology, 39(8), pp.100-103.

[5] Liu K, Xu W, Wu H, et al. (2023). Weighted hybrid order total variation model using structure tensor for image denoising. Multimedia Tools and Applications, 82(1), pp.927-943.

[6] Li M M, Li B Z. (2021). A novel weighted total variation model for image denoising. IET image processing, 15(12), pp.2749-2760.

[7] Golbaghi F K, Eslahchi M R, Rezghi M. (2021). Image denoising by a novel variable-order total fractional variation model. Mathematical Methods in the Applied Sciences, 44(8), pp.7250-7261.

[8] Zhang H, He Z, Wang X. A Novel Mesh Denoising Method Based on Relaxed Second-Order Total Generalized Variation. SIAM Journal on Imaging Sciences, 2022, 15(1): 1-22.

[9] Li X, Huang T Z, Zhao X L, et al. (2021). Adaptive total variation and second-order total variation-based model for low-rank tensor completion. Numerical Algorithms, 86(1), pp.1-24.

[10] ZHANG H Y, PENG Q C. (2006). Total variational adaptive image denoising model. Photoelectric Engineering, 33(3), pp.50-53.

[11] Bredies K, Kunisch K, Pock T. (2010). Total Generalized Variation. Siam Journal on Imaging Sciences, 3(3), pp.492-526.

[12] You Y L, Kaveh M. (2017). Fourth-order partial differential equations for noise removal. IEEE Transactions on Image Processing, 9(10), pp.1723-1730.

[13] Chen Y, He W, Yokoya N, et al. (2019). Hyperspectral image restoration using weighted group sparsity regularized low rank tensor decomposition. IEEE Transactions on Cybernetics, 50(8), pp.3556-3570.

[14] Li M M, Li B Z. (2022). A novel weighted anisotropic total variational model for image applications. Signal, Image and Video Processing, 16(1), pp.211-218.

[15] Khan A, Jin W, Naqvi R A. (2022). Perceptual adver-

sarial non-residual learning for blind image denoising. Soft computing: A fusion of foundations, methodologies and applications, 26(16), pp.7933 -7957.

[16] LEI Y, LIU S Q, ZHANG L Y, LIU T, ZHAO J. (2022). Summary of synthetic aperture radar image denoising based on deep learning. Journal of Ordnance Equipment Engineering, 43(11), pp. 71-80.

[17] YIN S Y, TANG Q. (2021). Adaptive image denoising model based on partial differential equations. Science and Technology Notification, 37(4), pp. 83-87.

[18] Yin X, Zhou S. (2015). Image Structure-Preserving Denoising Based on Difference Curvature Driven Fractional Nonlinear Diffusion. Mathematical Problems in Engineering, 6(1), pp. 1-16.

[19] FU L J, YAO Y, FU ZH L. (2014). Medical image filtering method combining median filtering with anisotropic diffusion. Computer Application, 34(1), pp. 145-148.

[20] YU J H, WANG Y Y. (2011). Summary of image noise reduction algorithms based on anisotropic diffusion. Journal of Electronic Measurement and Instruments, 25(02), pp. 105-116.

Author Biographies

SHI Zhenting is now a M.Sc. candidate at Nanjing University of Information Science and Technology. Her main research interest includes digital image processing.

E-mail: szt19981026@163.com

ZHOU Xianchun (Corresponding author) received Ph.D. from Nanjing University of Information Science and Technology in 2011. Now he is a professor and M.Sc. supervisor at Nanjing University of Infomation Science and Technology, is also a senior member of China Electronics Society. His main research interests include signal and information processing.

E-mail: zhouxc2008@163.com